

# Effects of Variation of Quantum Well Numbers on Gain Characteristics of Type-I InGaAsP/InP Nano-heterostructure

S. G. Anjum<sup>1</sup>, Sandhya K.<sup>2</sup>, A. B. Khan<sup>3</sup>, A. M. Khan<sup>4</sup>, M. J. Siddiqui<sup>5</sup>, P. A. Alvi<sup>\*6</sup>

<sup>1,3,5</sup>Department of Electronics Engineering, Aligarh Muslim University, Aligarh-202002, U.P., India

<sup>2,6</sup>Department of Physics, Banasthali Vidyapith-304022, Rajasthan, India

<sup>4</sup>Department of Electronics & Communication Engineering, Integral University, Lucknow-226026, UP, India

\*Corresponding author, e-mail: drpaalvi@gmail.com

## Abstract

*This paper reports the effects of variation of number of quantum wells in material gain characteristics and lasing wavelength of step index separately confined type-I InGaAsP/InP lasing nano-heterostructure for different carrier concentrations at room temperature in TE (Transverse Electric) mode of polarization. Peak material gain is found to be highest when the number of quantum well is one in the structure. However, for the case of 3QWs, 5QWs and 7QWs, it is almost same at a particular carrier density. Lasing wavelength at peak material gain considerably increases as the number of quantum well layers vary from single quantum well layer to three quantum well layers in the active region and after that it will remain almost same by any further increase in number of quantum wells for a particular carrier density. Furthermore, negative gain condition in the material gain spectra exists in the case of multiple quantum wells only at carrier concentration of  $2 \times 10^{18}/\text{cm}^3$ . The results suggest that the proposed nano-heterostructure is highly suitable as a light source in fiber optic links for long distance communication.*

**Keywords:** optical gain, nano-heterostructure, Semiconductor laser, quantum well laser, InGaAsP/InP

## 1. Introduction

The nano-scale heterostructures have played an important role in the area of optoelectronics, particularly, in optical fiber communication where long wavelengths are required for communication purpose. For more than half a century, the research in semiconductor lasers and lasing heterostructures has been continued and contributed in a great way in the area of optoelectronics [1-18]. For example, radiation properties of semiconductor laser such as directivity, beam brightness, and its narrow spectral width, and coherence compelled them the best light sources in fiber optic links for long distance communication. This has made the optical fibers commercial [17]. Over the time, long haul system capacity demands have been grown continuously, as has the requirement to improve the quality of semiconductor laser diode. In reply, quantum well laser diodes with maximum possible narrow width of the spectra (about tenths of a nanometer) have been designed. Various designs have been proposed, most of them were just disappeared, and only a few continue as useful products. Within the last twenty years there has been increasing attention in materials with nano-scale dimensions. Drastic advancement in the development of nano-scale crystal growth and device fabrication technologies has impelled the downscaling of semiconductor laser diodes, a trend also inspired by the need to attain larger color range, higher material gain, and lower lasing threshold [12], [15], [17]. Progress in material growth technologies, especially molecular beam epitaxy (MBE), metal-organic CVD, and a suite of chemical synthesis procedures, cause high quality nano-scale semiconductor structures fabrication possible [3], [9], [17]. Applying heterojunctions in semiconductor lasers was first suggested in 1963 when Herbert Kroemer, a well-known scientist in this domain, proposed the concept that population inversion could be greatly enhanced by integrating heterojunctions in the semiconductor laser structure [10]. For the material science of heterostructure fabrication, it took several years to meet with Kroemer's ideas but now it is acceptable as industry standard. Subsequently, it was noticed that the band gap energy could be controlled by utilizing the benefits of the quantum size effects in quantum well heterostructure. To make lasing action further effective, an especially thin active region, about 4

to 20 nm thicknesses, is designed by a particular fabrication technique [17]. Such semiconductor devices are named as quantum well laser diodes. The quantum well approach alters the density of energy levels possible for electrons and holes and results a much higher optical gain. The major benefits of a quantum well laser diode is more effective current-to-light conversion capability, better output beam confinement, and the ability to radiate a range of wavelengths [11], [17-18]. From a practical viewpoint, these benefits of the quantum well structure drastically lessen the threshold current and enhance the possibility of varying radiating wavelengths by changing the width of an active layer [17]. The main difficulty with the simple quantum well laser diode is that the thin layer is generally too small to efficiently confine the light. To rectify this problem, two more layers are added on, over the first three layers. These layers have a smaller index of refraction as compared to the center layer, and hence confine the light efficiently. Such a device is known as a separately confined heterostructure based semiconductor laser diode. Since the 1990s, about all commercial semiconductor laser diodes have been separately confined heterostructure based quantum well laser diodes. Commercially attractive wavelength range (0.5–4 $\mu$ m) may be comprised by most of the heterojunction designs fabricated from compound semiconductor III–V quaternary alloys, Especially, AlGaInP, InGaAlAs, AlGaAsSb, InGaAsP, InGaAsSb and InPAsSb [12], [15], [17]. The aforementioned quaternary alloys cover almost all ternary alloys from III–V elements. Due to the absence of knowledge about the dependence of various material parameters on the composition of the alloy has restricted a systematic progress to the design of custom-made optoelectronic devices. Quantum well laser diodes are possible with the following configurations: single quantum well (SQW), multiple quantum well (MQW), step-index separate confinement heterostructure (STINSCH) and graded-index separate confinement heterostructure (GRINSCH). A multiple quantum well laser can exhibit up to 100 mW powerful radiation [17]. Recent advances comprise strained quantum well based active media. By incorporating a controlled strain in an active layer, a designer can control the widths of the quantum well and the potential barrier. This results in the prospect of improving the semiconductor laser diode properties: controlling its wavelength, reducing its threshold current, and enhancing laser efficiency. Nowadays, in the field of nano-optoelectronics, the nano-scale lasing heterostructures having multiple quantum well have been most widely utilized [3], [7], [13]. The material system InGaAsP/InP based multiple quantum well lasing nano-heterostructures is generally utilized in optical fiber communications as a source of light because of their suitable lasing wavelength ranges. The quaternary compound semiconductor InGaAsP is a versatile laser material grown on InP substrates [1-2], [4]. Now a days, the separately confined heterostructures have been proposed as a vital element of the quantum well lasing heterostructures. A separately confined heterostructure with single quantum well, where the InGaAsP active region is the core layer of a five layered dielectric slab waveguide have already been reported [1-2], [4], [14]. The InGaAsP active layer is sandwiched by an InGaAsP layer on each side for better carrier confinement. The two outer InGaAsP material layers confine the optical field [1-2], [4], [8], [16]. A quaternary compound semiconductor material, Indium gallium arsenide phosphide (In<sub>1-x</sub>Ga<sub>x</sub>As<sub>y</sub>P<sub>1-y</sub>) is an alloy of indium phosphide and gallium arsenide. Previously mentioned compound semiconductor has uses in photonic devices, because of the ability to customize its band gap through variations in the alloy mole fractions, x and y. InP material based photonic integrated circuits, generally use In<sub>1-x</sub>Ga<sub>x</sub>As<sub>y</sub>P<sub>1-y</sub> to make quantum well layers, waveguides and other photonic structures, which is lattice matched to an Indium Phosphide substrate, facilitating single crystal epitaxial growth onto Indium Phosphide.

## 2. Theoretical Details

The optical gain coefficient in terms of photonic energy or transition wavelength can be simulated by the following expression;

$$G(E') = \frac{q^2 |M_B|^2}{E' \epsilon_0 m_0^2 c h n_{eff} W} \sum_{i,j} \int_g^{E_{gb}} m_{r,ij} C_{ij} A_{ij} (f_c - f_v) L(E) dE \quad (1)$$

The symbols used in the above expression for the material gain have been described in detail in references [5, 6]. In the above expression,  $E_{fc}$  and  $E_{fv}$  are the quasi-Fermi levels and can be related with the carrier concentrations by the following equations:

$$N = \frac{m_n^* kT}{\pi \hbar^2 L_z} \sum_i \ln \left[ 1 + e^{\frac{(E_{fc} - E_i)}{kT}} \right] \tag{2}$$

$$P = \frac{m_{hh}^* kT}{\pi \hbar^2 L_z} \sum_i \ln \left[ 1 + e^{\frac{(E_{fv} - E_{hi})}{kT}} \right] + \frac{m_{lh}^* kT}{\pi \hbar^2 L_z} \sum_i \ln \left[ 1 + e^{\frac{(E_{fv} - E_{li})}{kT}} \right] \tag{3}$$

where  $N$  and  $P$  are the electron and hole carrier concentration in the conduction and valence bands respectively;  $m_n^*$ ,  $m_{hh}^*$  and  $m_{lh}^*$  are the effective masses of the electrons, heavy holes and light holes respectively;  $L_z$  is the width of quantum well;  $\hbar$  is the reduced plank constant and  $k$  is the Boltzmann constant.

**3. Structural Details**

The schematic semiconductor layer structure and schematic energy band diagram used in the simulation is shown in Figure 1 and Figure 2 respectively. The proposed step index separately confined lasing nano-heterostructure comprises of a single quantum well layer of  $\text{In}_{0.9}\text{Ga}_{0.1}\text{As}_{0.59}\text{P}_{0.41}$  material of thickness 60 Å placed in between two wide bandgap barrier layers of material  $\text{In}_{0.75}\text{Ga}_{0.25}\text{As}_{0.55}\text{P}_{0.45}$  of thickness 50 Å followed by cladding layers of material  $\text{In}_{0.5}\text{Ga}_{0.5}\text{As}_{0.11}\text{P}_{0.89}$  of thickness 100 Å. Since the bandgap energy of quaternary compounds depend on alloy composition therefore bandgap energy of quaternary compound semiconductor,  $\text{In}_{1-x}\text{Ga}_x\text{As}_y\text{P}_{1-y}$  is different for different value of mole fraction  $x$ . Off course quantum well region bandgap is lesser as compare to that of barrier and barrier region bandgap is lesser as compare to that of cladding. The entire structure is fully grown on Indium phosphide substrate as given in Figure 1. Simulation has also been carried out for different quantum well numbers in the active region at different carrier densities.

$\text{In}_{1-x}\text{Ga}_x\text{As}_y\text{P}_{1-y}$ Cladding Layer x=0.50, y=0.11
$\text{In}_{1-x}\text{Ga}_x\text{As}_y\text{P}_{1-y}$ Barrier Layer x=0.25, y=0.55
$\text{In}_{1-x}\text{Ga}_x\text{As}_y\text{P}_{1-y}$ Quantum well Layer x=0.10, y=0.59
$\text{In}_{1-x}\text{Ga}_x\text{As}_y\text{P}_{1-y}$ Barrier Layer x=0.25, y=0.55
$\text{In}_{1-x}\text{Ga}_x\text{As}_y\text{P}_{1-y}$ Cladding Layer x=0.50, y=0.11
InP Substrate

Figure 1. Schematic layer diagram of step index separate confinement SQW based InGaAsP/InP lasing nano-heterostructure

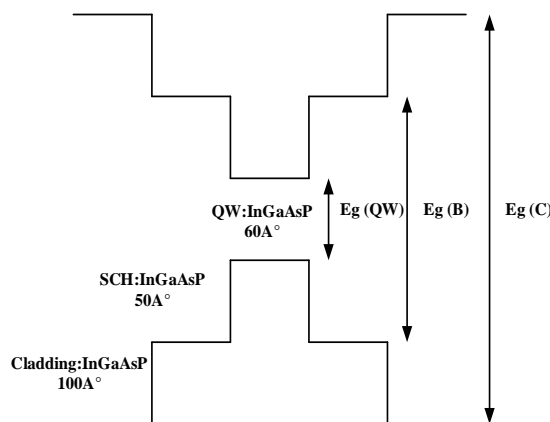


Figure 2. Schematic energy band structure of step index separate confinement SQW based InGaAsP/InP lasing nano-heterostructure

Simulation study of a compressively strained quantum well lasers with a 750 $\mu\text{m}$  ridge length and 3 $\mu\text{m}$  ridge width for four distinct number of quantum wells in active region at four different carrier densities are done using GAIN software package. The strain level is chosen such as to adjust the bandgap energy to generate laser output having a range of wavelength in between 1.2  $\mu\text{m}$  to 1.7  $\mu\text{m}$ . Material compositions of quantum well regions and barrier regions are chosen such as to achieve lattice matched condition, but the substrate selection is done in such a manner that the quantum well layers are compressively strained by 1.2 % in amount, and hence, suitable selection of the substrate is very much required for compressively strained structure.

#### 4. Results and Discussion

Simulation study of material gain as a function of lasing wavelength and photon energy for step index separate confinement InGaAsP/InP nano-heterostructure by varying the number of quantum wells 1QW, 3QWs, 5QWs & 7QWs in the active region for four different carrier densities  $2 \times 10^{18}/\text{cm}^3$ ,  $4 \times 10^{18}/\text{cm}^3$ ,  $6 \times 10^{18}/\text{cm}^3$ , and  $8 \times 10^{18}/\text{cm}^3$  in TE mode of polarization at temperature 300 K and is thoroughly summarized in Table 1.

In Figure 3, photon energy dependent material gain is calculated at carrier density of  $2 \times 10^{18}/\text{cm}^3$  for different quantum well numbers and is found that peak gain of 2230.14/cm occurs at 0.867eV photon energy for single quantum well structure. Presence of spikes in the material gain spectra or abrupt change in the material gain that appears because of some nonlinearity, an aftereffect of transient response of the optical beam in the proposed lasing nano-heterostructure. Furthermore, at carrier density of  $2 \times 10^{18}/\text{cm}^3$  a negative material gain or material loss exists above a certain value of photon energy and below the corresponding wavelengths in the gain spectra which indicates optical loss because of the absorption of light within the waveguide for the case of multiple quantum well in the active region as shown in Figure 3 and Figure 4. While there is no negative material gain condition occurring at carrier densities of  $4 \times 10^{18}/\text{cm}^3$ ,  $6 \times 10^{18}/\text{cm}^3$ ,  $8 \times 10^{18}/\text{cm}^3$  for multiple quantum well structure. However in the case of single quantum well structure there is no any material loss found at any aforementioned carrier densities. Similarly, in Figure 4, wavelength dependent material gain is plotted at carrier concentration of  $2 \times 10^{18}/\text{cm}^3$  for different quantum well numbers and is found that peak gain of 2230.14/cm attains at 1.4297  $\mu\text{m}$  wavelengths for single quantum well structure. In the same way in Figure 5, photon energy dependent material gain is computed at carrier concentration of  $4 \times 10^{18}/\text{cm}^3$  for different quantum well numbers and is found that peak gain of 4164.97/cm reaches at 0.8689eV photon energy again for single quantum well structure.

Table 1. Numerical Data for InGaAsP/InP heterostructure with Different Number of Quantum

No. of quantum wells	1QW	3QWs	5QWs	7QWs
Photon energy/Lasing wavelength at peak material gain	(peak material gain)	(peak material gain)	(peak material gain)	(peak material gain)
Photon energy at peak material gain for carrier density of $2 \times 10^{18}/\text{cm}^3$	0.8672 eV (2230.14/cm)	0.85348 eV (1129.469/cm)	0.8519198 eV (1058.209/cm)	0.85113 eV (1034.97/cm)
Lasing wavelength at peak material gain for carrier density of $2 \times 10^{18}/\text{cm}^3$	1.4297 $\mu\text{m}$ (2230.14/cm)	1.45287 $\mu\text{m}$ (1129.469/cm)	1.45553 $\mu\text{m}$ (1058.209/cm)	1.4568 $\mu\text{m}$ (1034.95/cm)
Photon energy at peak material gain for carrier density of $4 \times 10^{18}/\text{cm}^3$	0.8689 eV (4164.97/cm)	0.854769 eV (2791.82/cm)	0.853598 eV (2767.93/cm)	0.852818 eV (2760.53/cm)
Lasing wavelength at peak material gain for carrier density of $4 \times 10^{18}/\text{cm}^3$	1.427 $\mu\text{m}$ (4164.97/cm)	1.45068 $\mu\text{m}$ (2791.82/cm)	1.45267 $\mu\text{m}$ (2767.93/cm)	1.4540 $\mu\text{m}$ (2760.53/cm)
Photon energy at peak material gain for carrier density of $6 \times 10^{18}/\text{cm}^3$	0.86407 eV (5481.94/cm)	0.85308 eV (3999.2558/cm)	0.852304 eV (3990.118/cm)	0.8515244 eV (3987.496/cm)
Lasing wavelength at peak material gain for carrier density of $6 \times 10^{18}/\text{cm}^3$	1.4350 $\mu\text{m}$ (5481.94/cm)	1.453548 $\mu\text{m}$ (3999.2558/cm)	1.4548789 $\mu\text{m}$ (3990.118/cm)	1.4562118 $\mu\text{m}$ (3987.497/cm)
Photon energy at peak material gain for carrier density of $8 \times 10^{18}/\text{cm}^3$	0.8608249 eV (6342.549/cm)	0.85378 eV (4959.2169/cm)	0.855349 eV (4980.98/cm)	0.855349 eV (4968.81/cm)
Lasing wavelength at peak material gain for carrier density of $8 \times 10^{18}/\text{cm}^3$	1.440478 $\mu\text{m}$ (6342.549/cm)	1.452349 $\mu\text{m}$ (4959.2169/cm)	1.4497 $\mu\text{m}$ (4980.98/cm)	1.4497 $\mu\text{m}$ (4968.81/cm)

Furthermore, in Figure 6, lasing wavelength dependent material gain is analyzed at carrier concentration of  $4 \times 10^{18}/\text{cm}^3$  for different quantum well numbers and is found that peak

gain of 4164.97/cm occurs at 1.427  $\mu\text{m}$  again for single quantum well configuration. However, in Figure 7, photon energy dependent material gain is obtained at carrier density of  $6 \times 10^{18}/\text{cm}^3$  and is found that peak gain of 5481.94/cm attains at 0.8640eV photon energy. But in Figure 8, lasing wavelength dependent material gain curve is plotted at carrier concentration of  $6 \times 10^{18}/\text{cm}^3$  and is found that peak gain of 5481.94/cm occurs at the wavelength of 1.4350  $\mu\text{m}$ . Furthermore, in Figure 9, photon energy dependent material gain curve is drawn at carrier concentration of  $8 \times 10^{18}/\text{cm}^3$  for different quantum well numbers and is found that peak material gain of 6342.549/cm achieves at the photon energy of 0.8608 eV. Also, in Figure 10, wavelength dependent material gain is computed at carrier concentration of  $8 \times 10^{18}/\text{cm}^3$  for different quantum well numbers and is found that peak material gain of 6342.549/cm reaches at 1.440478  $\mu\text{m}$ . Moreover, quasi Fermi levels of conduction band electrons and valence band holes are plotted in Figure 11 and Figure 12 respectively for different quantum well numbers in the nano-heterostructure. In conduction band, it ranges from 0.011 eV to 0.23 eV for single quantum well, from -0.005 eV to 0.214 eV for 3QWs, from -0.009 eV to 0.21 eV for 5QWs and from -0.01 eV to 0.209 eV for 7QWs and But in valence band, it ranges from -0.099 eV to 0.034 eV for single quantum well, from -0.114 eV to 0.0139 eV for 3QWs, from -0.114 eV to 0.0138eV for 5QWs and from 0.114 eV to 0.0137 eV for 7QWs.

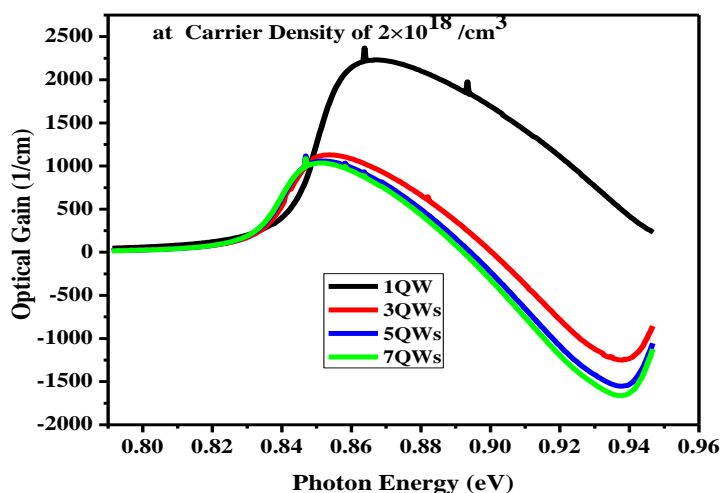


Figure 3. Optical gain as a function of photon energy

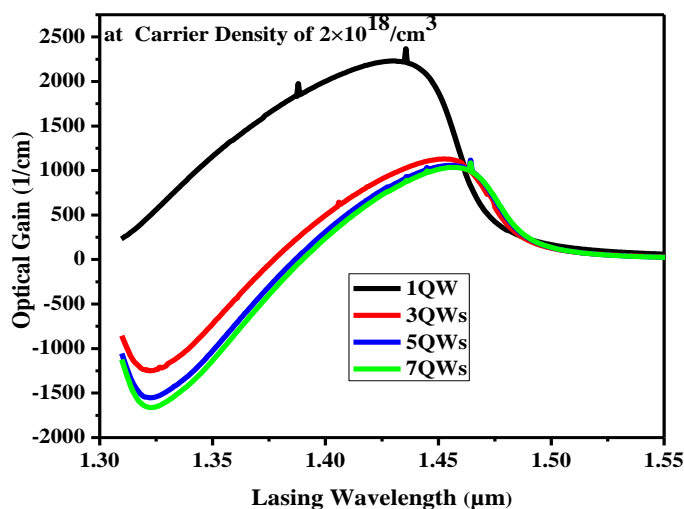


Figure 4. Optical gain as a function of lasing wavelength

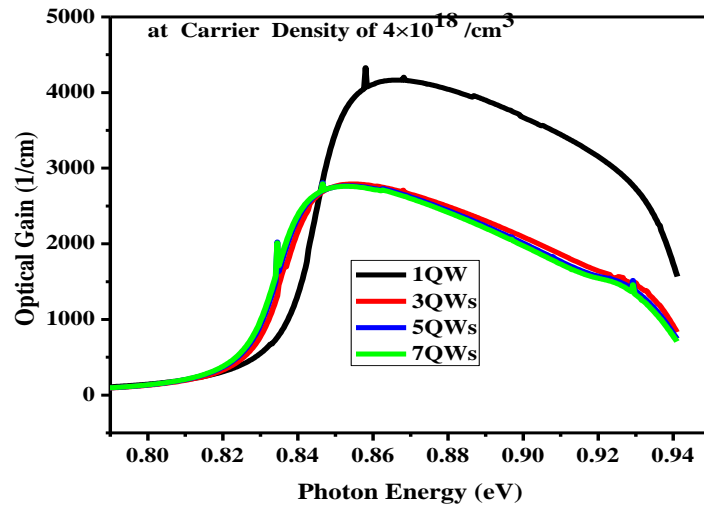


Figure 5. Optical gain as a function of photon energy

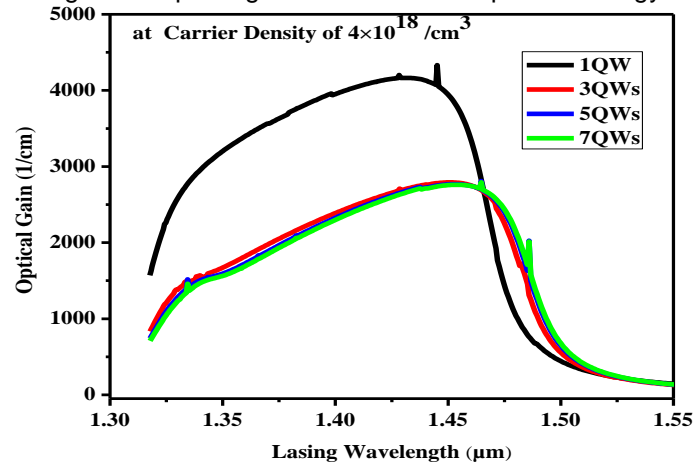


Figure 6. Optical gain as a function of lasing wavelength

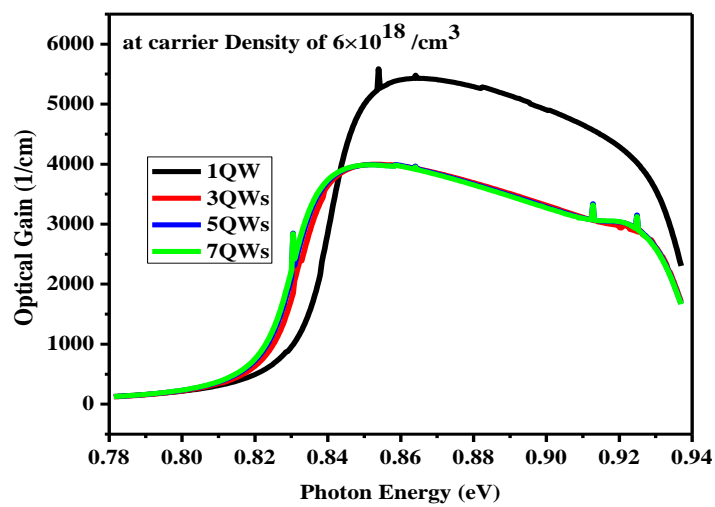


Figure 7. Optical gain as a function of photon energy

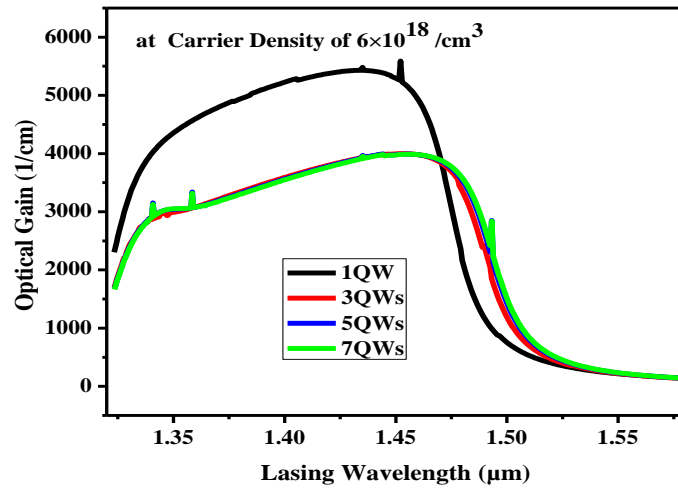


Figure 8. Optical gain as a function of lasing wavelength

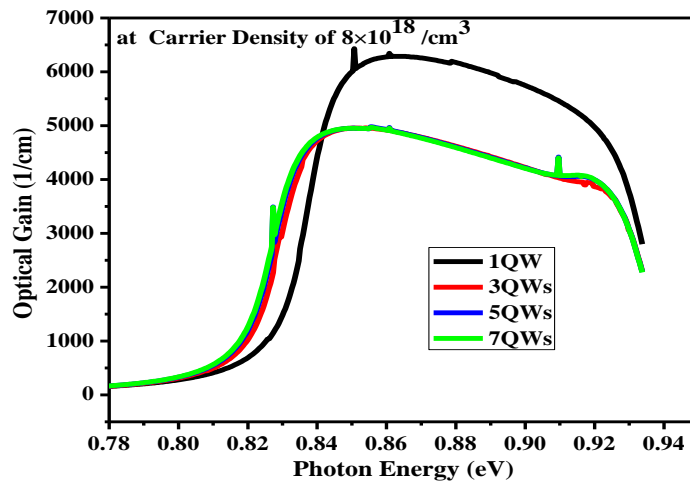


Figure 9. Optical gain as a function of photon energy

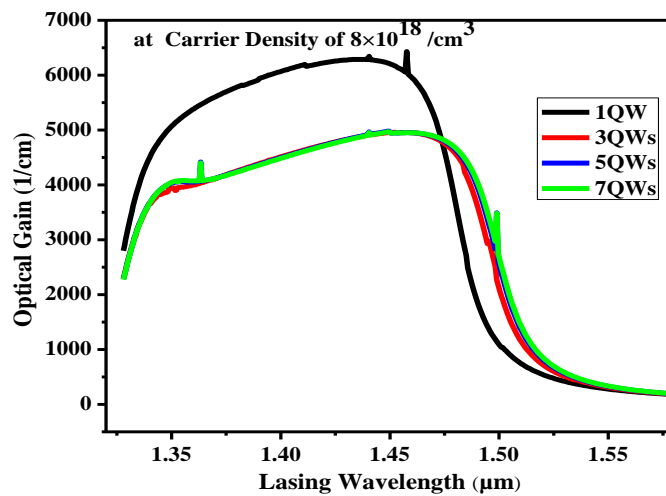


Figure 10. Optical gain as a function of lasing wavelength

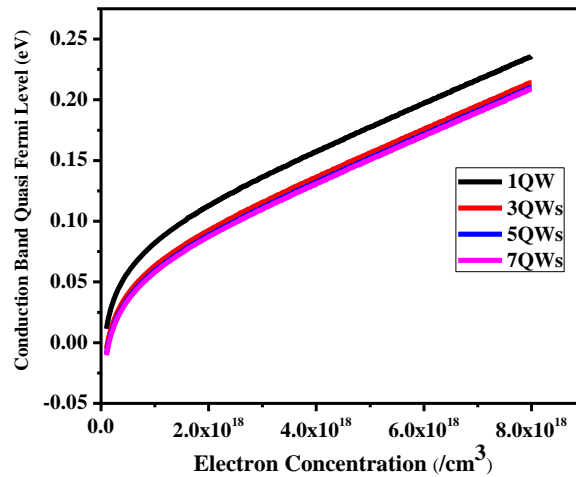


Figure 11. Quasi Fermi level in conduction band

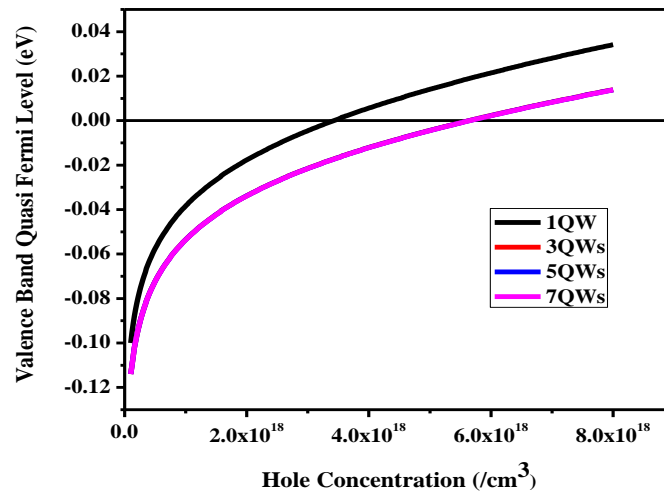


Figure 12. Quasi Fermi level in valance band

In Figure 13, peak material gain and lasing wavelength as a function of quantum well numbers for four different carrier densities are computed and is found that overall peak material gain of 6342.549/cm achieves at 1.44  $\mu\text{m}$  lasing wavelength for carrier concentration of  $8 \times 10^{18}/\text{cm}^3$  in single quantum well based lasing nano-heterostructure. Lasing wavelength at peak material gain increases as we increase the number of quantum wells for carrier densities of  $2 \times 10^{18}/\text{cm}^3$ ,  $4 \times 10^{18}/\text{cm}^3$  and  $6 \times 10^{18}/\text{cm}^3$ . While at carrier density of  $8 \times 10^{18}/\text{cm}^3$ , lasing wavelength at peak material gain initially increases when number of quantum well changes from single quantum well to three quantum wells after that it slightly decreases and remains approximately same for the case of 5QWs & 7QWs. Consequently, photon energy at peak material gain decreases as we increase the number of quantum wells at carrier densities of  $2 \times 10^{18}/\text{cm}^3$ ,  $4 \times 10^{18}/\text{cm}^3$ , and  $6 \times 10^{18}/\text{cm}^3$ . While at carrier density of  $8 \times 10^{18}/\text{cm}^3$ , photon energy at peak material gain initially decreases when number of quantum well changes from single quantum well to three quantum wells after that it slightly increases and remains approximately same for the case of 5QWs & 7QWs. Hence lasing wavelength at peak material gain increases considerably as the number of quantum well vary from single quantum well to three quantum wells in the active region and after that it remains almost same by any further increase in number of quantum wells for a particular carrier density.

Also, peak material gain is found to be almost same for the case of 3QWs, 5QWs and 7QWs at a particular carrier density but for the case of single quantum well it is highest.

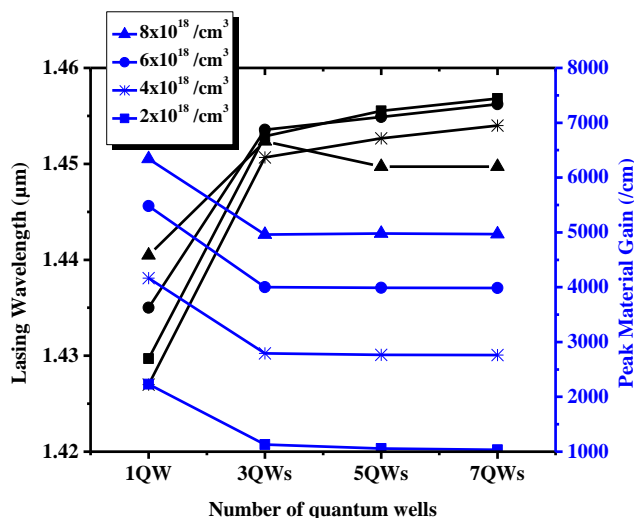


Figure 13. Peak material gain and Lasing wavelength as a function of number of quantum wells for different carrier densities

## 5. Conclusion

For step index separately confined type-I InGaAsP/InP nano-heterostructure, material gain as a function of lasing wavelength and photon energy in TE polarization mode at temperature 300K for various number of quantum wells 1QW, 3QWs, 5QWs & 7QWs in the active region for four different carrier densities  $2 \times 10^{18}/\text{cm}^3$ ,  $4 \times 10^{18}/\text{cm}^3$ ,  $6 \times 10^{18}/\text{cm}^3$ ,  $8 \times 10^{18}/\text{cm}^3$  have been thoroughly studied and it is found that overall peak material gain of  $6342.55/\text{cm}^3$  occurs at  $1.44 \mu\text{m}$  wavelength and  $0.86 \text{ eV}$  photon energy for carrier density of  $8 \times 10^{18}/\text{cm}^3$  of single quantum well nano-heterostructure. Furthermore, negative gain condition in the material gain spectra occurred only at lower carrier concentration of  $2 \times 10^{18}/\text{cm}^3$  but at the higher carrier densities of  $4 \times 10^{18}/\text{cm}^3$ ,  $6 \times 10^{18}/\text{cm}^3$ ,  $8 \times 10^{18}/\text{cm}^3$ , there is no any material loss in the case of multiple quantum wells in the active region of the structure. However, in the case of single quantum well structure there is no any material loss found at any aforementioned carrier densities. Also, peak material gain is found to be almost same for the case of 3QWs, 5QWs and 7QWs at a particular carrier density but for the case of single quantum well it is highest. But lasing wavelength at peak material gain considerably increases as we increase the number of quantum wells from single quantum well to three quantum wells in the active region after that it remains almost same by any further increase in quantum well numbers for a particular carrier density.

## Acknowledgement

Authors are thankful to the Research Lab of Electronics Engineering Department, A.M.U, Aligarh, India under UGC-SAP scheme supported by DSA-I program. Authors are also grateful to Dr. Tso-Min Chou, Deptt. of Electrical Engg, S.M.U, Dallas, Texas for his technical help.

## References

- [1] R Yadav, P Lal, F Rahman, S Dalela, PA Alvi. Well Width Effects on Material Gain and Lasing Wavelength in InGaAsP/InP Nano-Heterostructure. *Journal of Optoelectronics Engineering*. 2014; 2(1): 1-6.
- [2] R Yadav, M Sharma, S Jha, P Lal, M J. Siddiqui, F Rahman, S Dalela, PA Alvi. Investigation of Gain Characteristics of GRIN InGaAsP/InP Nano-Heterostructure. *Indian Journal of Pure & Applied Physics*. 2015; 53: 447-455.

- [3] SG Anjum, MJ Siddiqui. Multiple Quantum Well Based Lasing Nanostructures: A Review. *IMPACT*. 2013; 278-282, DOI: 10.1109/MSPCT.2013.6782135.
- [4] R Yadav, P Lal, F Rahman, S Dalela, PA Alvi. Investigation of Material Gain of  $\text{In}_{0.90}\text{Ga}_{0.10}\text{As}_{0.59}\text{P}_{0.41}/\text{InP}$  Lasing Nano-Heterostructure. *International Journal of Modern Physics B*. 2014; 28(10). 1450068, DOI: 10.1142/S0217979214500684.
- [5] P Lal, S Dixit, S Dalela, F Rahman, PA Alvi. Gain Simulation of Lasing Nano-Heterostructure  $\text{Al}_{0.10}\text{Ga}_{0.90}\text{As}/\text{GaAs}$ . *Physica E: Low-dimensional systems and Nanostructures*. 2012; 46: 224-231.
- [6] P Lal, R Yadav, F Rahman, PA Alvi. Carrier Induced Gain Simulation of  $\text{InGaAlAs}/\text{InP}$  Nano-Heterostructure. *Advanced Science, Engineering and Medicine*. 2013; 5(9): 918-925(8).
- [7] M Sharma, R Yadav, P Lal, F Rahman, PA Alvi. Modal Gain Characteristics of Step SCH  $\text{InGaP}/\text{GaAs}$  MQW Based Nanoscale Heterostructures. *Advances in Microelectronic Engineering (AIME)*. 2014; 2(2).
- [8] JC Yong, JM Rorison, IH White. 1.3  $\mu\text{m}$  Quantum Well  $\text{InGaAsP}$ ,  $\text{AlGaInAs}$ , and  $\text{InGaAsN}$  Laser Material Gain: A Theoretical Study. *IEEE J. Quantum Electron*. 2002; 38(12): 1553–1564.
- [9] JJ Coleman. The Development of the Semiconductor Laser Diode after the First Demonstration in 1962. *Semiconductor Science and Technology*. 2012; 27: 10. 090207.
- [10] H Kroemer. A Proposed Class of Heterojunction Injection Lasers. *Proc. IEEE*. 1963; 51: 1782-1783.
- [11] N Holonyak Jr, RM Kolbas, RD Dupuis, PD Dapkus. Quantum Well Heterostructure Lasers. *IEEE J. Quantum Electron*. 1980; 16(2): 170.-186
- [12] SL Chuang. Physics of Photonic Devices. Second edition, *John Wiley & Sons*, New York, (2009).
- [13] W Yang, Q Y Ping, P J Qing, Z L Juan, Z H Liang, W Wei. High Characteristic Temperature  $\text{InGaAsP}/\text{InP}$  Tunnel Injection Multiple-Quantum-Well Lasers. *CHIN. PHYS. LETT*. 2010; 27(11).
- [14] T Namegaya, N Matsumoto, N Yamanaka, N Iwai, H Nakayama, A Kasukawa. Effects of Well Number in 1.3- $\mu\text{m}$   $\text{GaInAsP}/\text{InP}$  GRIN-SCH Strained-Layer Quantum-Well Lasers. *IEEE Journal of Quantum Electronics*. 1994; 30(2): 578-584.
- [15] P Bhattacharya. Semiconductor Optoelectronic Devices. NJ: Prentice Hall. 1996.
- [16] LM Dolginov, AE Drakin, PG Eliseev, BN Sverdlov, EG Shevchenko. CW  $\text{InGaAsP}/\text{InP}$  Injection Lasers with Very Low Threshold Current Density at Room Temperature. *IEEE Journal of Quantum Electronics*. 1985; QE-21(6).
- [17] DK Mynbaev, LL Scheiner. Fiber-Optic Communications Technology. Pearson Education Inc., ISBN 978-81-7758-418-9 (2009).
- [18] DS Chemla, A Pinczuk. Introduction to the Special Issue on Physics and Applications of Semiconductor Quantum Well Structures. *IEEE Journal of Quantum Electronics*. 1986; QE-22(9): 1609.